



Using integrated GC-MS analysis, *in vitro* experiments, network pharmacology: exploring migao fatty oil active components/mechanisms against coronary heart disease

Lina JIAN^{1#}, Jiangtao GUO^{1#}, Yongping ZHANG^{1,2,3}, Jie LIU^{1,2,3*} , Yao LIU¹, Jian XU^{1,2,3*} 

Abstract

Coronary heart disease (CHD) is one of the main diseases causing morbidity and mortality globally, with oxidative damage and lipid peroxidation associated with oxidative stress and atherosclerosis. *Cinnamomum migao* is a Miao ethnomedicine that has been shown to provide relief from CHD symptoms. A gas chromatograph-mass spectrometer (GC-MS) was used to determine the chemical components of ten batches of migao fatty oil (MFO), yielding a total of 35 chemical constituents. The antioxidant activity of MFO *in vitro* was assessed using the DPPH· and ABTS·⁺ assay methods, and both indicated good antioxidant activity. The network pharmacology predicted the active constituents of MFO and their therapeutic influence on the mechanism of oxidative damage-induced coronary heart disease (OD-CHD). Six compounds were discovered in MFO, including tau-cadinol acetate and dodecanoic acid, which may play a role in OD-CHD by acting on lipids and atherosclerosis, the PI3K-Akt signalling pathway, and other pathways. In conclusion, our study lays the foundation for investigating the use of MFO in the treatment of OD-CHD.

Keywords: migao fatty oil; oxidative damage-induced coronary heart disease; antioxidant activity; network pharmacology; *in vitro* experiments.

Practical Application: Migao fatty oil exerts preventive effects on coronary heart disease.

1 Introduction

In recent years, an increasing number of scientists have concentrated on investigating free radicals and redox pathways towards assisting in the prevention of cardiovascular disease, tumours, and other diseases and ageing (Hu et al., 2021; Liang et al., 2021; Panov & Dikalov, 2020). The free radicals in the cells of the human body are in a dynamic balance under normal conditions, and are continuously produced in the human body, resulting from pollution, radiation, sunlight exposure, and other factors. Because the body's antioxidant defence system cannot destroy them, excessive generation of free radicals damages cellular proteins, lipids, and DNA, causing cell necrosis and apoptosis (Ullah et al., 2017). Antioxidants are thus a critical component of the body's defence against oxidative damage (Gatasheh et al., 2021; Chen et al., 2021; Halliwell et al., 2021). They trap and neutralize free radicals, hence preventing free radical harm to the human body (Halliwell, 2020). Finding high-efficiency, low-toxicity, and reasonably priced antioxidants from natural medicines and foods has thus become an important direction of research in this field.

Coronary heart disease (CHD) is a highly prevalent cardiovascular disease with increasing morbidity and mortality as the population ages. There is much evidence suggesting that

oxidation plays a key role in the progression of atherosclerosis at all stages (Zhong et al., 2019). Fatty acids, present in fatty oils, have special lipophilic and electron-stabilizing properties that make them a promising class of natural medical antioxidants (Sherratt & Mason, 2018). By quickly forming less harmful free radical compounds, protein free radical damage can be rapidly repaired, avoiding the emergence of cascades of new reactive species and therefore avoiding atherosclerosis and coronary heart disease (Gebicki & Nauser, 2021).

Migao is the dry ripe fruit of *Cinnamomum migao* H.W.Li which belongs to the *Cinnamomum* Trew family of Lauraceae. Migao can be soaked in water and eaten like kimchi, and it can also be used for seasoning in cooking. Both methods have a similar function of strengthening the spleen-stomach. The fruit can also be broken or powdered and ingested for heart pain in China, which can instantly ease the pain. Migao, according to Hmong medicine, is able to warm middle-jiao to dispel colds, regulate qi, and relieve pain. Migao may protect against acute myocardial ischemia injury by boosting antioxidant efficacy, according to modern pharmacological investigations. However, its antioxidant activity mechanism has yet to be acknowledged (Li & Yang, 2021). Researchers discovered that MFO has the

Received 27 Aug., 2022

Accepted 01 Oct., 2022

¹School of Pharmacy, Guizhou University of Traditional Chinese Medicine, Guiyang, China

²National Engineering Research Center of Miao's Medicines, Guiyang, China

³Guizhou Chinese Medicine Processing and Preparation Engineering Technology Research Center, Guiyang, China

*Corresponding author: xiaojie0716@126.com; Xujiangzy123@163.com

#Lina Jian and Jiangtao Guo share senior authorship.

ability to treat CHD, but the chemical composition of MFO was unknown and there was no standardised antioxidant test technique.

Despite significant developments in CHD, such as interventional and surgical therapy, the issue of providing effective and safe care to patients with circulatory failure caused by CHD is still a topic of conversation. Creating bioactive foods with several compositions is another means, in addition to creating medications to treat CHD, that may be used at various phases of the disease's development. This approach not only serves as a preventive precaution for those who have no clinical symptoms of the condition but also encourages the development of food treatment, which may be combined with medication or surgery.

To learn more about MFO's chemical composition and mechanism of action in the treatment of OD-CHD, we used a gas chromatograph-mass spectrometer (GC-MS) to analyse the compositions of 10 batches of MFO; we then used network pharmacology and molecular docking technology to predict the pharmacodynamic material basis and mechanism of MFO in the treatment of OD-CHD from a molecular perspective; simultaneously, the DPPH method and the ABTS⁺ assay methods were employed to assess the *in vitro* antioxidant capabilities of MFO in order to develop a more acceptable test method for fatty oil antioxidants (Figure 1). The goal of this research is to establish a theoretical foundation for fully using Migao medicinal material resources, as well as to create the groundwork to produce Guizhou-area-specific medicinal material.

2 Materials and methods

2.1 Materials and reagents

Ten batches of migao were identified as the dry ripe fruit of *Cinnamomum migao* H.W.Li by Professor Sun Qingwen of

Guizhou University of Traditional Chinese Medicine (Table 1). The reagents used were 1,1-diphenyl-2-trinitrophenylhydrazine (DPPH, purity $\geq 97.0\%$), Tihibu (Shanghai) Chemical Industry Development Co., Ltd.; Diammonium 2,2'-azino-bis(3-ethylbenzothiazoline-6-sulfonate) (ABTS, purity $\geq 98.0\%$), Hefei Bomei Biotechnology Co., Ltd.; potassium persulfate, potassium hydroxide, hexanes, sodium hydroxide, hydrochloric acid, methanol, ethanol absolute, petroleum ether (30-60 °C) and were all of analytical grade, plus homemade distilled water.

2.2 Analysis of Chemical Composition of MFO

Preparation of MFO

Extraction of MFO

MFO was extracted by the Soxhlet extractor method. The extraction solvent was petroleum ether, the ratio of material to liquid (g/mL) was 1: 15, and the temperature was 85 °C for the extraction. The extract was transferred to a weighing bottle

Table 1. Source information of *Cinnamomum migao*.

S/N	Latin name	Market address
S1	<i>Litsea lancilimba</i>	Luodian, Guizhou
S2	<i>Litsea lancilimba</i>	Luodian, Guizhou
S3	<i>Litsea lancilimba</i>	Luodian, Guizhou
S4	<i>Litsea lancilimba</i>	Cheheng, Guizhou
S5	<i>Litsea lancilimba</i>	Cheheng, Guizhou
S6	<i>Litsea lancilimba</i>	Anlong, Guizhou
S7	<i>Litsea lancilimba</i>	Gongli, Guizhou
S8	<i>Litsea lancilimba</i>	Tiane, Guangxi
S9	<i>Litsea lancilimba</i>	Tiane, Guangxi
S10	<i>Litsea lancilimba</i>	Wangmo, Guizhou

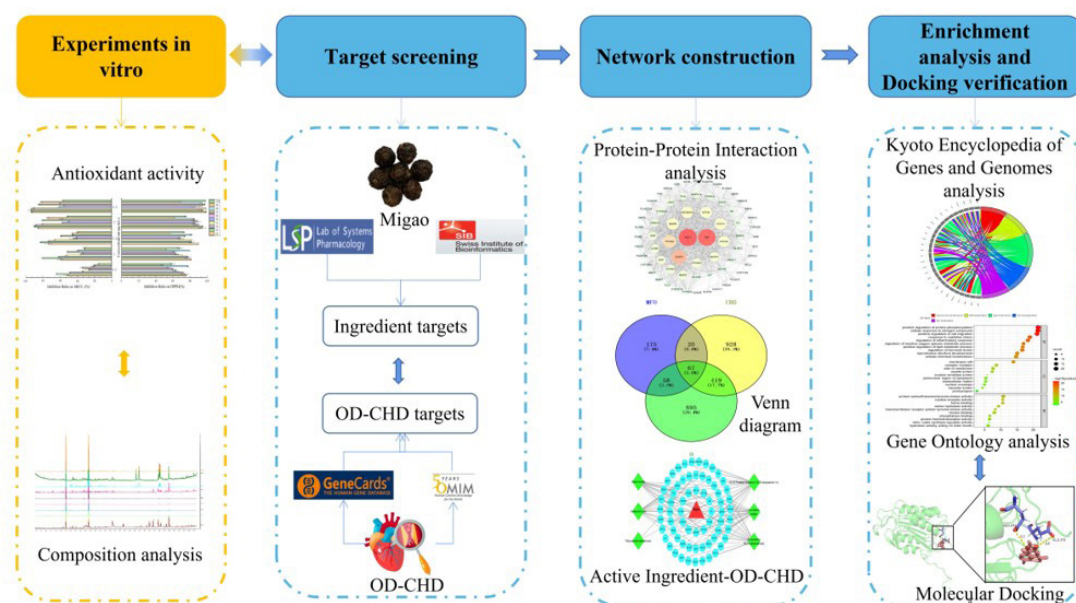


Figure 1. Integrated workflow for discovery of the potential mechanisms of MFO against OD-CHD.

after passing through a rotary evaporator, and dried in an oven at 105 °C for 1 h to obtain the MFO.

Preparation of methyl esterified MFO

To accurately weighed MFO (0.50 g) was added 20 mL of 0.5 mol/mL potassium hydroxide-methanol solution, then placed it in a 60 °C water bath for 15 min, and removed to cool. Thereafter, 40 mL of 25% hydrochloric acid was added, placed in a 60 °C water bath for 15 min, and then removed to cool. Another 20 mL of n-hexane was added and mixed well. Finally, 20 mL of saturated sodium hydroxide was added and left to stand for 15 min. The supernatant was evaporated to dryness under reduced pressure to obtain methyl esterified MFO (Huang et al., 2020).

GC-MS analysis conditions

GC-MS was performed on an Agilent HP6890/5975C GC-MS (USA) to profile the chemical composition of each MFO. GC was equipped with an Rtx-5 MS(30 m×0.25 mm×0.25 μm) capillary column. Temperature programming: the column temperature was 100 °C, rose to 130 °C at the rate of 3 °C/min and then at 2 °C/min to 230 °C for 2 min. Running time 60 min. Vaporization chamber temperature 230 °C. The carrier gas was high purity helium (99.999%). The precolumn pressure was 18.49 psi, the carrier gas flow was 1.0 mL/min, the split ratio was 10:1, and the solvent delay time was 5.5 min. The ion source was an EI source, and its temperature was 230 °C; electron energy 70 eV. Emission current 34.6 μA; multiplier voltage 1953 V; the interface temperature was 280 °C; and the mass ranged from 50 to 500 amu.

Analysis of the composition of MFO

After obtaining mass spectral information from GC-MS, it was matched against the NIST 17 database. The peak area normalization method was used to express its relative percentage.

2.3 Determination of antioxidant activity

Preparation of MFO solutions

The MFO sample under 2.2.1 above, was prepared ensuring sample solutions with a mass concentration of 0.5, 1, 1.5, 2.0, 2.5 mg·mL⁻¹ using absolute ethanol.

DPPH ((2,2-Diphenyl-1-picrylhydrazyl)) free radical scavenging assay

The antioxidant activity of MFO was measured in terms of radical scavenging ability, using a DPPH plant assay. All measurements were performed as follows: an amount of 1.0 mL of the five different concentrations of liquid extract was added to 2.0 mL of the DPPH· ethanol solution with a mass concentration of 0.1 mmol L⁻¹, and the absorbance readings were taken after 30 min against the blank at 517 nm (Zhang et al., 2022b; Nie et al., 2022). The antioxidant capacity was calculated using the following Equation 1 where, (Ac: the absorbance of DPPH· solution and solvent, Ai: the absorbance of the sample

solution and DPPH· solution, Aj: the absorbance of solvent solution and the sample):

$$\text{Radical Scavenging Capacity (\%)} = \frac{Ac - (Ai - Aj)}{Ac} \times 100\% \quad (1)$$

ABTS·⁺ (2,2'-azinobis-(3-ethylbenzothiazoline-6-sulphonate) free radical scavenging assay

ABTS·⁺ solution (7 mmol/L) and potassium persulfate solution (2.45 mmol/L) should be mixed in equal amounts. The reaction system was placed at room temperature and sheltered from light for 24 hours, diluted with anhydrous ethanol, the absorbance set at 734 nm (Jovanović et al., 2021; Aljobair, 2022), and the wavelength was 0.70 (± 0.002). In this way, the ABTS·⁺ working solution was obtained. All measurements were performed as follows: the amount of 2.0 mL of liquid extract was added to 2.0 mL of the ABTS·⁺ working solution, and the absorbance readings were taken after 6 min at 734 nm. The antioxidant capacity was calculated using the following Equation 2 (A_{Sample} - the absorbance of the sample and ABTS·⁺ working solution, A_{Blank} - the absorbance of ABTS·⁺ working solution and solvent, A_{Control} - the absorbance of solvent solution and the sample)

$$\text{Radical Scavenging Capacity} = \frac{A_{\text{Blank}} - (A_{\text{Sample}} - A_{\text{Control}})}{A_{\text{Blank}}} \times 100\% \quad (2)$$

2.4 Network pharmacology analysis predicts mechanism of oxidation resistance

Screening of active ingredients of MFO

To obtain the active chemical ingredients, we used the Traditional Chinese Medicine Systems Pharmacology Database and Analysis Platform (TCMSP) to screen the chemical components under section 2.2 above. Its screening conditions were oral bioavailability (OB) ≥ 30% and drug-likeness index (DL) ≥ 0.18 (Liu et al., 2022); or we used PubChem to obtain the 2D structure or Canonical Smiles information of the chemical components, and imported the information into the SwissADME database (<http://www.swissadme.ch/>) for screening (Oh et al., 2021). The filter conditions were that the (gastro-intestinal) GI absorption value was “high”, and the five amounts under Drug-likeness were “Yes”

Prediction of the active ingredient target of MFO

The Canonical Smiles of active ingredient were entered into the SwissTargetPrediction database (<http://www.swisstargetprediction.ch/>), and the species was defined as “homo sapiens”, followed by a probability > 0 screening (Zhu et al., 2022). It was merged with the predicted targets of the TCMSP database corrected by the UniProt database (<https://www.uniprot.org/>), and the target genes of the MFO's active components were obtained after deduplication.

OD-CHD related targets gene screening

Using “Oxidation damage” and “Coronary Heart Disease” as the search keywords, we searched the GeneCards database (<https://www.gene-cards.org/>) (Yu et al., 2022), and OMIM

database (<http://www.omim.org>) (Wang et al., 2022b), to obtain potential targets associated with OD-CHD. The two disease database targets were combined and the repeat value was deleted to get the OD-CHD related targets.

Interaction network of component-target

We used the Venny 2.1.0 online mapping tool to draw a Venn diagram of the potential targets of the active ingredients of MFO and OD-CHD related targets, and to obtain the intersection targets of MFO and OD-CHD. The intersection targets were imported into Cytoscape 3.8.2 software to construct an interaction network of component targets.

Protein-Protein Interaction (PPI) network and core target genes

The common targets of MFO and OD-CHD were imported into the STRING database (<http://string-db.org/>) (Li et al., 2022), and the targets with interaction confidence greater than 0.4 were selected. Import it into Cytoscape 3.8.2 software to get PPI visualization network diagram. Finally, with the help of the “CytoHubba” plug-in of the software, the top 5 target genes were obtained, which were the core target genes.

Gene Ontology (GO) and Kyoto Encyclopedia of Genes and Genomes (KEGG) analysis

Using the Metascape database (<http://metascape.org/>), GO functional annotation and KEGG pathway enrichment analysis were performed on the intersection target genes of MFO and OD-CHD, and $p < 0.01$ was used as the screening condition (Wei et al., 2022). The enrichment results were displayed using the SRplot (<http://www.bioinformatics.com.cn/srplot>).

Molecular docking verification

Six active ingredients were selected for molecular docking with the five key target genes. Pre-processing the protein receptor molecule was performed by using the Py MOL software after having downloaded the 3D structures of major possible target proteins from the RCSB PDB library (<https://www.pdbus.org/>) (Wu et al., 2022). We downloaded the 3D structures of key potential target proteins from the RCSB PDB database (<https://www.pdbus.org/>), and used the Py MOL software to pre-process the protein receptor molecule (Sun et al., 2022). The pre-treatment of active compound ligands was performed using OpenBabelGUI software. We imported the pre-processed potential targets and active compound components into the docking software Auto Dock for molecular docking. With the help of Py MOL software, the compounds with a higher docking score and more stable conformation were combined with the target protein to perform molecular docking visualisation analysis (Zhang et al., 2022a).

3 Results

3.1 Composition analysis of MFO

In the ten batches of MFO, a total of 35 fatty acid components were identified. Among them, eight fatty acid components, with a relative percentage of 54.73%, were among the 38 components

that were isolated from S1. From S2 – S10 there were, respectively: S2 (relative percentage 85.75%), comprising 20 fatty acids from 53 components; S3 (91.73%), 11 fatty acids from 23 components; S4 (96.14%), eight fatty acids from 13 components; S5 (93.56%), five fatty acids from 10 components; S6 (96.01%), 9 fatty acids from 18 components; S7 (71.99%), eight fatty acids from 21 components; S8 (76.27%), 20 fatty acids from 67 components; S9 (88.98%), 4 fatty acids, from 7 components; and S10 (96.47%), 9 fatty acids from 14 components. There were 17 medium-chain fatty acids (MCFAs) and 18 long-chain fatty acids among the 35. The peak area normalization method was used to calculate the relative percentage content of each component (Table 2 and Figure 2.)

3.2 Antioxidant activity *in vitro*

Because antioxidant activity varied *in vitro*, each of the ten batches had its own response characteristics and processes. There was no benchmark that effectively represented all chemicals' antioxidant capacity in complicated systems. Consequently, the antioxidant activity of the ten batches of MFO was determined using the DPPH· and ABTS·⁺ techniques, as indicated in Figure 3. The antioxidant activity of these were positively linked with the mass concentration. S2 displayed high antioxidant activity, according to ABTS·⁺ technology, with a clearance rate of 64.56% - 94.29%. The results of the DPPH· technique demonstrated that S1 had high antioxidant activity, with a clearance rate of 75.88% - 98.87%. Furthermore, we discovered that the clearance rate obtained by the DPPH· approach was often higher than that obtained by the ABTS·⁺ method, which could be owing to the DPPH· reagent's lipophilicity. This meant that when determining

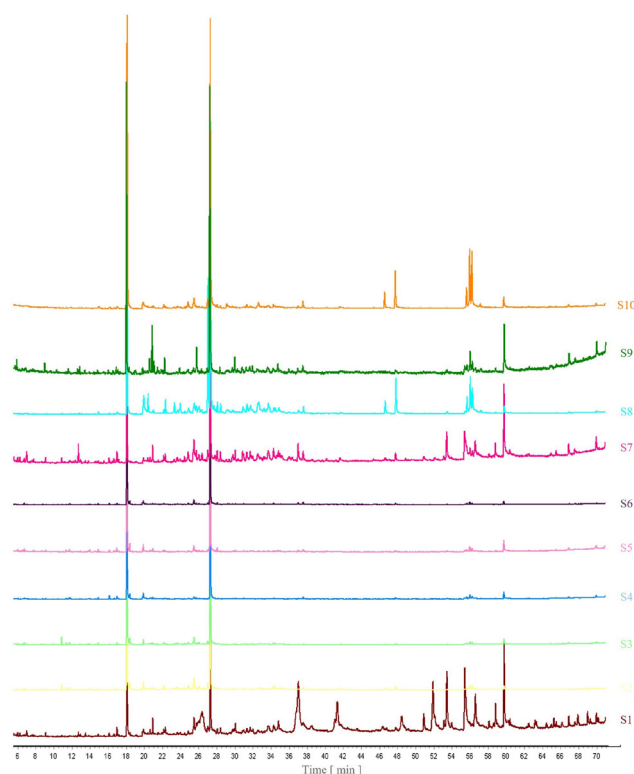


Figure 2. GC-MS profile of 10 batches of MFO compositions.

Table 2. Ten batches of MFO compositions (S1-S10) and relative percentage of constituents.

Compound Name	Formula	S ₁	S ₂	S ₃	S ₄	S ₅	S ₆	S ₇	S ₈	S ₉	S ₁₀
Thymol acetate	C ₁₂ H ₁₆ O ₂	0.52	0.23	0.39	0.53	0.61	0.33	1.31	0.19		
Methyl decanoate	C ₁₁ H ₂₂ O ₂	18.72	46.06	61.34	51.76	54.26	53.71	16.76	15.32	35.87	36.76
Methyl dodecanoate	C ₁₃ H ₂₆ O ₂	15.46	30.89	23.88	40.16	36.04	38.76	40.55	27.3	44	35.44
(R)-lavandulyl (R)-2-methylbutanoate	C ₁₅ H ₂₆ O ₂	0.61						1.48			
Guaiol acetate	C ₁₇ H ₂₈ O ₂	0.62						2	0.78	6.48	
Isovaleric anhydride	C ₁₀ H ₁₈ O ₃	4.68									
2-Methylbutanoic anhydride	C ₁₈ H ₂₂ O ₂	0.62									
5-tert-Butyl-2,2'-dimethoxy-biphenyl	C ₁₈ H ₂₂ O ₂	5.94						4.59			
4-Terpinenyl acetate	C ₁₂ H ₂₀ O ₂		0.06								
Methyl octanoate	C ₉ H ₁₈ O ₂		0.08								
Spirobicyclo[2.2.1]heptane-2,2'-(1,3'-dioxo-2'-oxocyclohex-5'-ene), 1,6,7,7-tetramethyl-	C ₁₄ H ₂₀ O ₃		0.75	1.54					0.07		
Neoisothujyl acetate	C ₁₂ H ₂₀ O ₂		0.29	0.33							
β-Terpinyl acetate	C ₁₂ H ₂₀ O ₂		0.24	0.17	0.23						
Geranyl propionate	C ₁₃ H ₂₂ O ₂		0.14								
α-Terpinyl acetate	C ₁₂ H ₂₀ O ₂		0.1					2.2	0.07		
Shisool formate	C ₁₁ H ₁₈ O ₂		0.2								
Bornyl formate	C ₁₁ H ₁₈ O ₂		1.56								
Tau-Cadinol acetate	C ₁₇ H ₂₈ O ₂		1.47	1.18					12.84		1.19
2,6,10-Trimethyl-12-acetoxy-2,6,10-dodecatriene-1-ol	C ₁₇ H ₂₈ O ₃		0.19								
Methyl tetradecanoate	C ₁₅ H ₃₀ O ₂		0.45		0.44		0.69		0.65		0.73
Methyl palmitoleate	C ₁₇ H ₃₂ O ₂		0.26						1.37		2.01
Methyl palmitate	C ₁₇ H ₃₄ O ₂		0.83				0.29		3.86		4.76
Methyl elaidate	C ₁₉ H ₃₆ O ₂		0.86	0.79	0.54	1.21	0.71		3.78	2.63	6.84
Methyl vaccenate	C ₁₉ H ₃₆ O ₂		0.6	0.57	0.99				2.71		6.44
Isobornyl formate	C ₁₁ H ₁₈ O ₂			0.31							
Borneol, trifluoroacetate (ester)	C ₁₂ H ₁₇ F ₃ O ₂			1.23	1.49	1.44	0.9				
Ethyl 1-Methylimidazole-2-carboxylate	C ₇ H ₁₀ N ₂ O ₂						0.26		0.17		
Decanoic acid	C ₁₀ H ₂₀ O ₂						0.36		2.78		
6-Octen-1-one, 3,7-dimethyl-3-ethenyl-1-(4-methoxyphenyl)-	C ₁₉ H ₂₆ O ₂	7.56						3.1			
Isothujyl acetate	C ₁₂ H ₂₀ O ₂								1.21		
Proximadiol	C ₁₅ H ₂₈ O ₂								0.99		
Lauric acid	C ₁₂ H ₂₄ O ₂								0.22		
γ-Eudesmol acetate	C ₁₇ H ₂₈ O ₂								0.27		
Methyl linoleate	C ₁₉ H ₃₄ O ₂		0.49						1.69		2.3
Methyl stearate	C ₁₉ H ₃₈ O ₂								0.2		

antioxidant activity *in vitro*, we could use a detection method that has features similar to the analyte.

We used the Manhattan Distance technique to perform cluster analysis and Pearson's correlation analysis on the MFO from various origins in order to investigate the relationship between common components and the antioxidant activity. The antioxidant activity measured by the DPPH· method was positively correlated with the contents of methyl decanoate and methyl dodecanoate, whereas the antioxidant activity measured by the ABTS·⁺ method was negatively correlated with the contents of methyl decanoate and methyl dodecanoate, as shown in Figure 4. The features of migao were similar that of DPPH· since the common components are all fatty acids before methyl esterification, indicating that the DPPH· approach was better for determining the antioxidant activity of fatty oils. Figure 5 showed that S1 (September 2018), S2 (September 2019), S4 (September

2019) were the same class; S3 (October 2019) was a solitary class; S7 (October 2020) and S9 (October 2020) were the same class; S5 (October 2019) and S6 (October 2020) were the same class; S8 (October 2020) and S10 (October 2020) were the same class; and the collection time of this classification was closely related.

3.3 Network pharmacology research

Active ingredients of MFO

TCMSP and SwissADME were used to screen the chemical compositions of 35 MFO under section "3.1" yielding a total of six MFO active ingredients (see Table 3).

Targets of active ingredients and OD-CHD

After sorting the prospective targets predicted by TCMSP and the SwissTargetPrediction website, a total of 320 potential

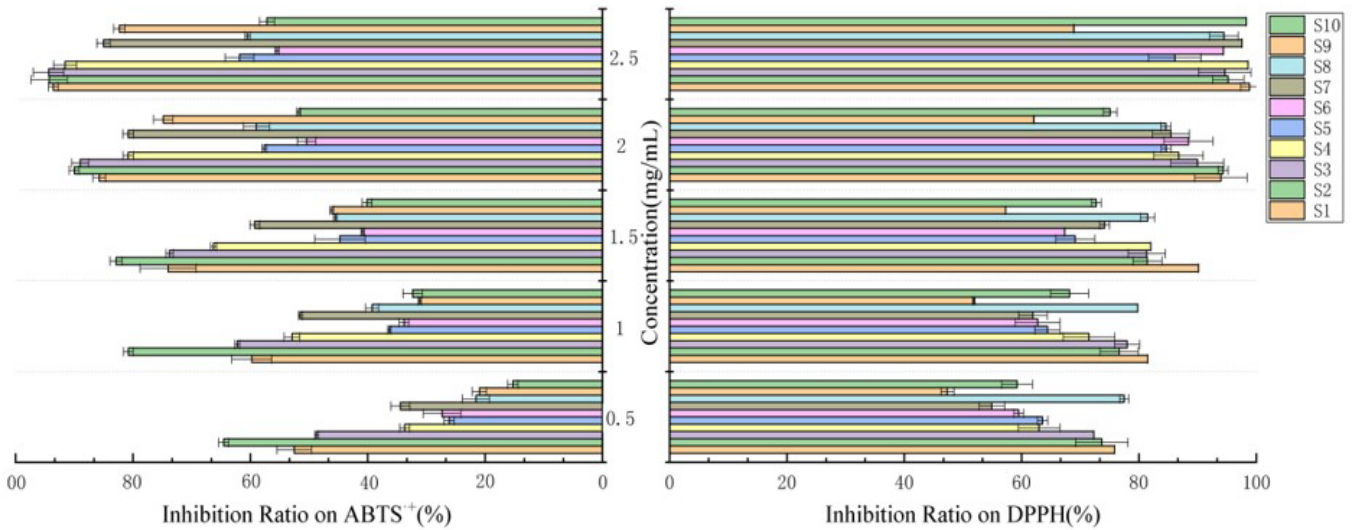


Figure 3. *In vitro* antioxidant results of 10 batches of MFO using different methods.

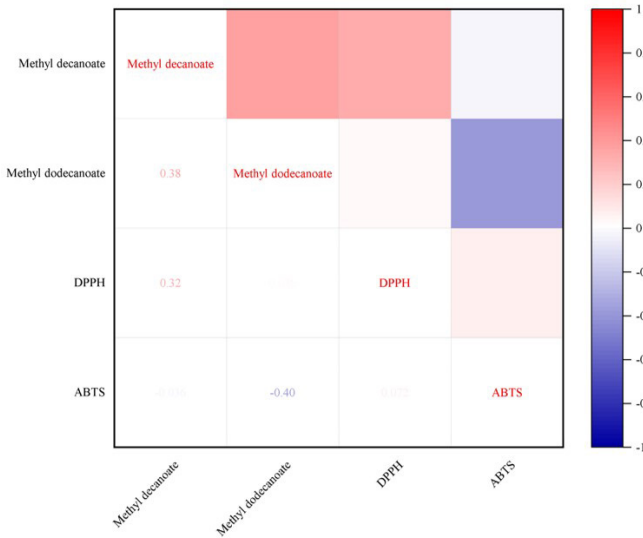


Figure 4. Results of Pearson correlation analysis.

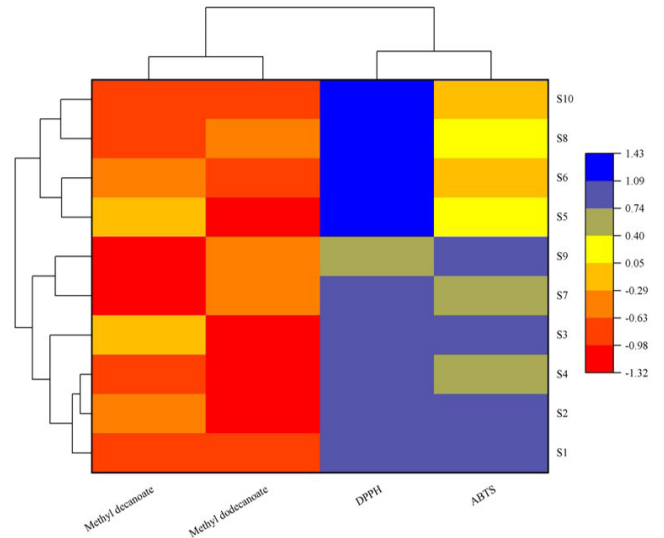


Figure 5. Results of cluster analysis with Manhattan Distance technique.

targets were found. Thereafter after sorting out the GeneCards and OMIM databases, 1239 OD-related targets and 1434 CHD-related targets were found. In total 67 target genes at the intersection of MFO and OD-CHD were discovered using the Venny 2.1.0 online drawing tool (Figure 6).

Construction of “active ingredients-targets-OD-CHD” network

MFO’s six active ingredients and the Venny online tool’s 67 intersecting targets were combined in Cytoscape 3.8.2 software to create an “active ingredient-target-OD-CHD” network, as illustrated in Figure 7. There were 94 nodes and 198 edges in the network. 2,6,10-trimethyl-12-acetoxy-2,6,10-dodecatriene-1-ol, tau-cadinol acetate, (R)-lavandulyl (R)-2-methylbutanoate, dodecanoic acid, guaiol acetate, and trifluoroacetyl-epiisoborneol could interact with 24, 22, 21, 19, 18 and 2 target proteins, respectively, based on the degree value.

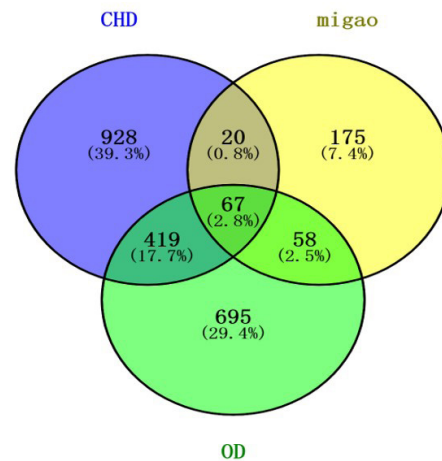
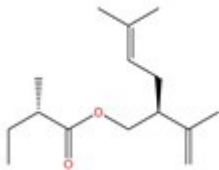
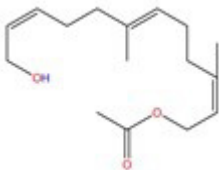
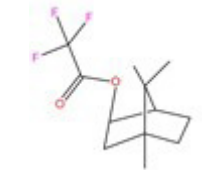
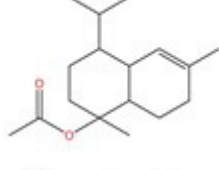
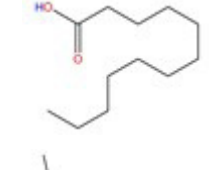
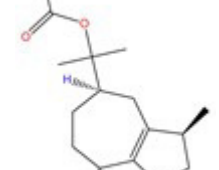


Figure 6. MFO and OD-CHD intersection target genes.

Table 3. Active ingredient information of MFO.

PubChemCID	Chemical composition	Molecular structure	Screening conditions			
			OB	DL	GI absorption	Druglikeness(Yes)
87232330	(R)-lavandulyl (R)-2-methylbutanoate		-	-	High	5
5363409	2,6,10-Trimethyl-12-acetoxy-2,6,10-dodecatriene-1-ol		-	-	High	5
564724	Trifluoroacetyl-epiisoborneol		-	-	High	5
14683249	Tau-Cadinol acetate		-	-	High	5
3893	Dodecanoic acid		23.59	0.04	High	5
240122	Guaiol acetate		-	-	High	5

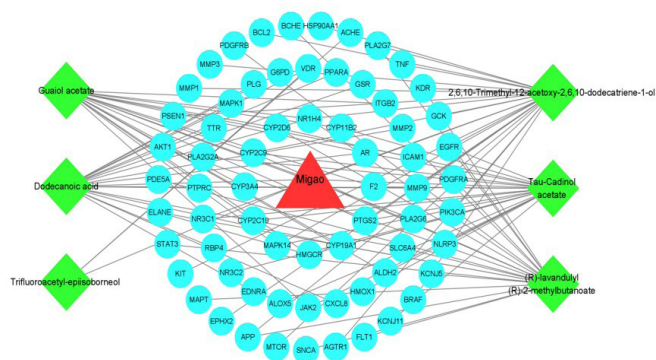


Figure 7. MFO “active ingredient-OD-CHD” network.

PPI network analysis

The STRING database (<http://string-db.org/>) was used to import the common targets of MFO and OD-CHD, and the results were shown using Cytoscape 3.8.2 software, as shown in Figure 8. The network included 67 nodes, which constituted 538 interaction relationships (in the network, the size and colour of nodes were positively correlated with the importance of nodes). Using the “CytoHubba” plugin, the top five target genes were AKT Serine/Threonine Kinase 1 (AKT1), Tumor Necrosis Factor (TNF), Epidermal Growth Factor Receptor (EGFR), Prostaglandin-Endoperoxide Synthase 2 (PTGS2), and Matrix Metalloproteinase 9 (MMP9), which were predicted to be closely related to OD-CHD.

GO and KEGG analysis

The intersection targets were added into the Metascape database, producing 5883 GO enrichment analysis results ($p < 0.01$), comprising 531 molecular functions, 4027 biological

processes, and 325 cellular components. The biological process included positive regulation of protein phosphorylation, cellular response to nitrogen compounds, positive regulation of cell migration, etc.; the cell composition included membrane raft, receptor complex, side of membrane, etc.; and the molecular functions included protein serine/threonine/tyrosine kinase activity, nuclear receptor activity, and heme binding, among other things. An SRplot was used to depict the top 10 enrichment results (Figure 9).

KEGG pathway enrichment analysis yielded a total of 239 entries ($p < 0.01$). Lipid and atherosclerosis, PI3K-Akt signalling pathway, Rap1 signalling pathway, MAPK signalling pathway, Fluid shear stress and atherosclerosis, and other pathways were involved in OD-CHD. The results of these five enrichments were visualized utilizing the SRplot platform (Figure 10).

Molecular docking verification

The top five core target genes of MFO and OD-CHD were selected for molecular docking with the top six active components of MFO, as shown in Table 4. The smaller the docking binding force value, the more stable the ligand-receptor binding was, and the greater the chance of interaction. Tau-Cadinol acetate had the lowest binding force to matrix metalloproteinase 9 (MMP9), with a value of $-7.06 \text{ kcal mol}^{-1}$ ($1 \text{ kcal} \approx 4.186 \text{ kJ}$). As demonstrated in Figure 11, components with low binding energies with proteins were chosen for the docking visualization.

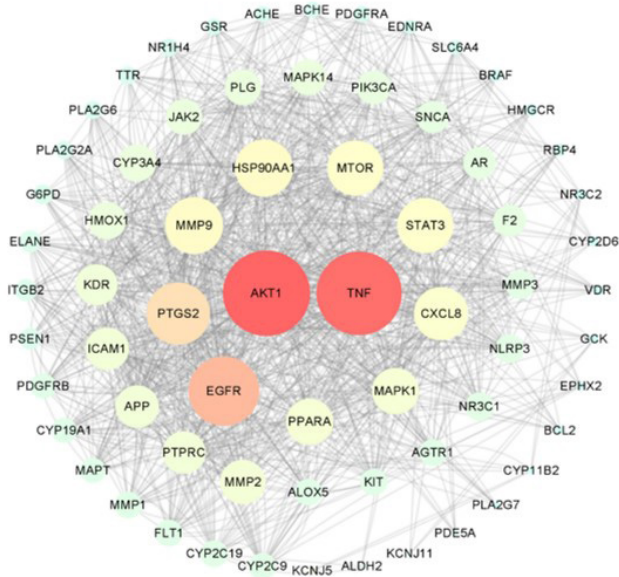


Figure 8. PPI network of target genes at the intersection of MFO and OD-CHD.

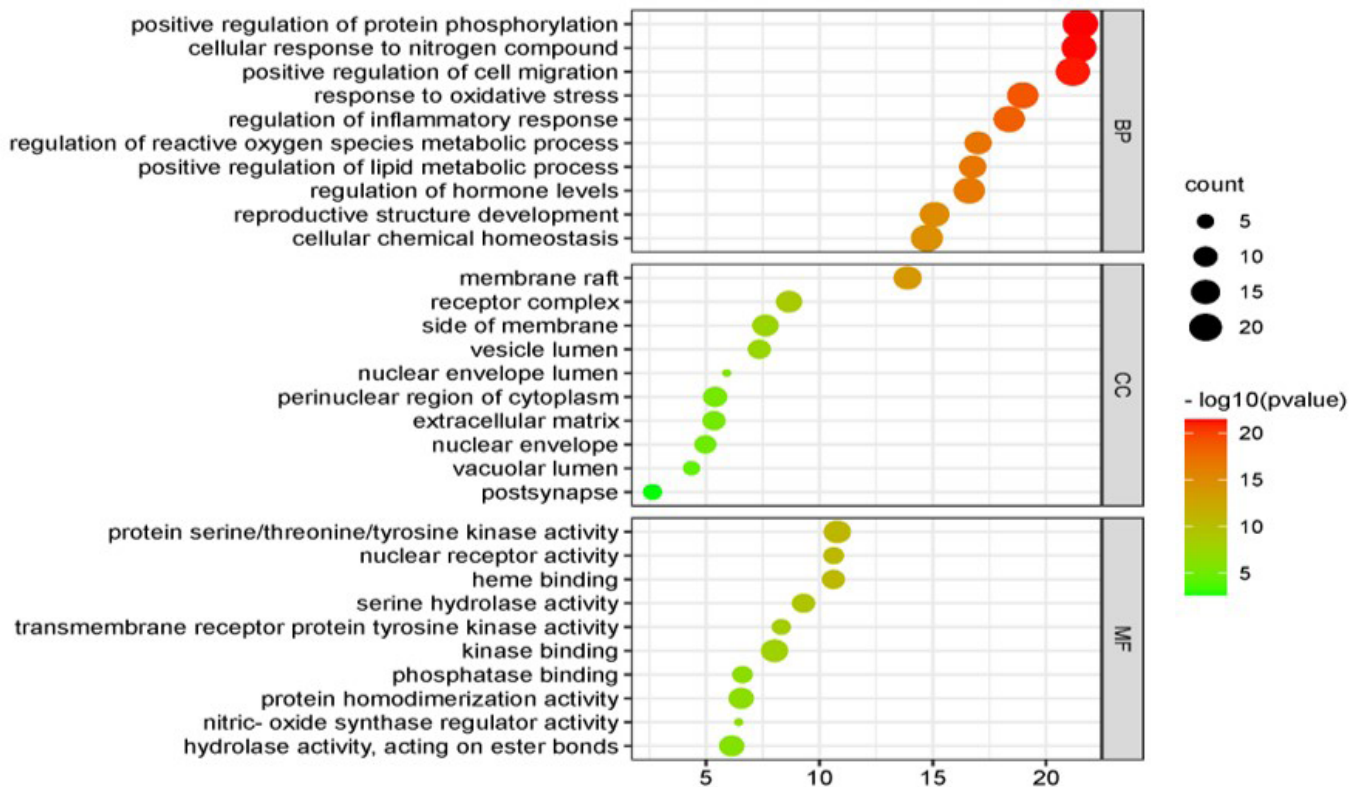


Figure 9. GO functional enrichment analysis bubble plot.

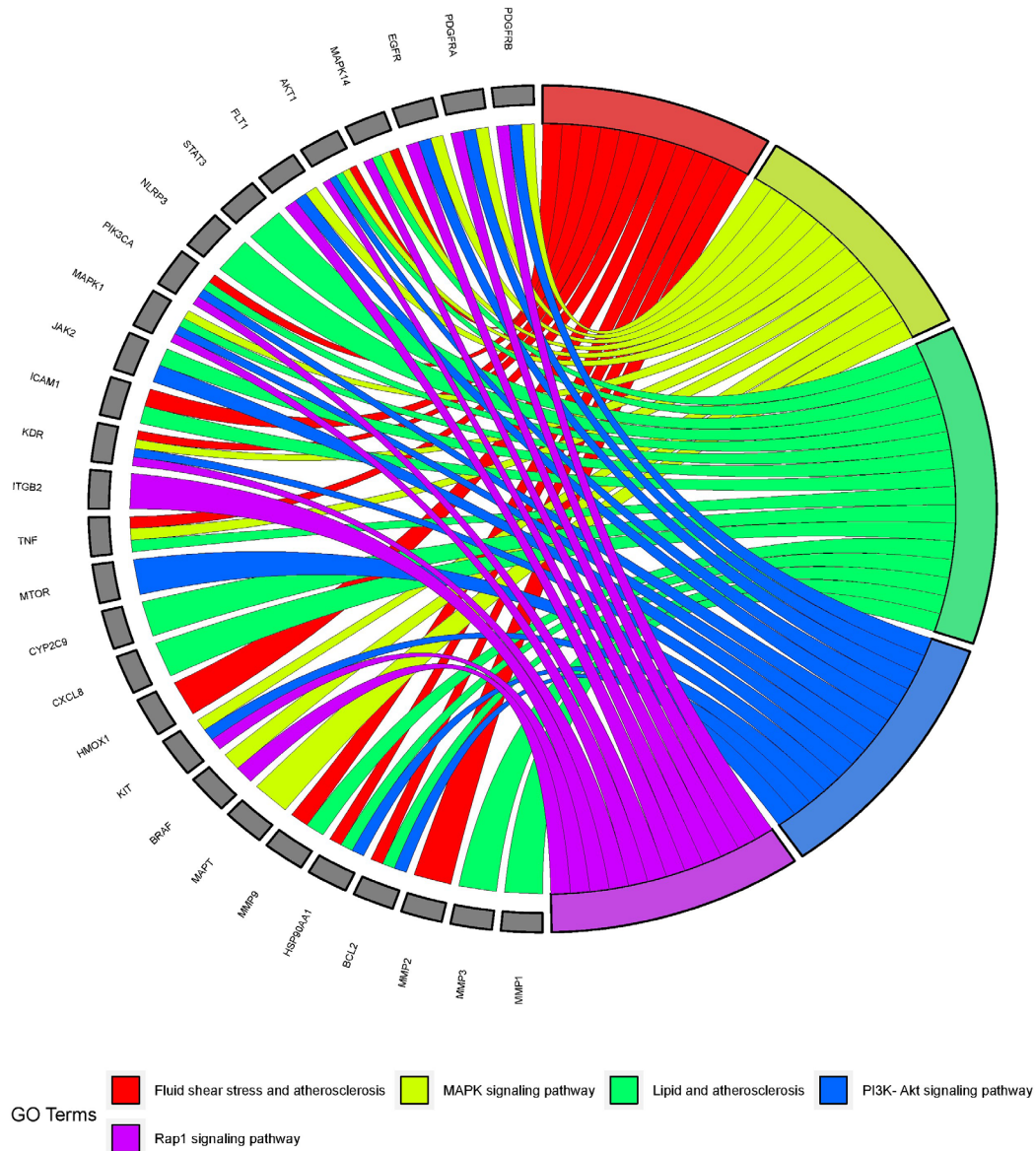


Figure 10. MFO “target-pathway” interaction network.

Table 4. Molecular docking results.

Active ingredient	Binding energy/kcal·mol ⁻¹				
	AKT1	TNF	EGFR	PTGS2	MMP9
2,6,10-trimethyl-12-acetoxy-2,6,10-dodecatriene-1-ol	-4.87	-4.00	-3.97	-3.12	-5.48
(R)-lavandulyl (R)-2-methylbutanoate	-3.74	-3.24	-3.09	-3.17	-4.97
tau-cadinol acetate	-5.35	-5.04	-4.55	-4.73	-7.06
dodecanoic acid	-3.25	-2.96	-3.27	-2.60	-3.73
guaiol acetate	-5.81	-5.51	-4.99	-4.89	-6.74
trifluoroacetyl-epiisoborneo	-4.92	-4.61	-4.49	-3.37	-5.36

4 Discussion

The antioxidant activity of 10 batches of MFO were examined *in vitro* in this study, and all showed good antioxidant activity. Increasing numbers of academics have focused on MCFAs in

recent years. MCFAs have been shown in studies to not only reduce myocardial oxidative damage, but also to be converted by the liver into ketone bodies as an alternative energy source to compensate for cardiac injury (Saifudeen & Renuka, 2021). The MCFAs, capric acid and dodecanoic acid have proved

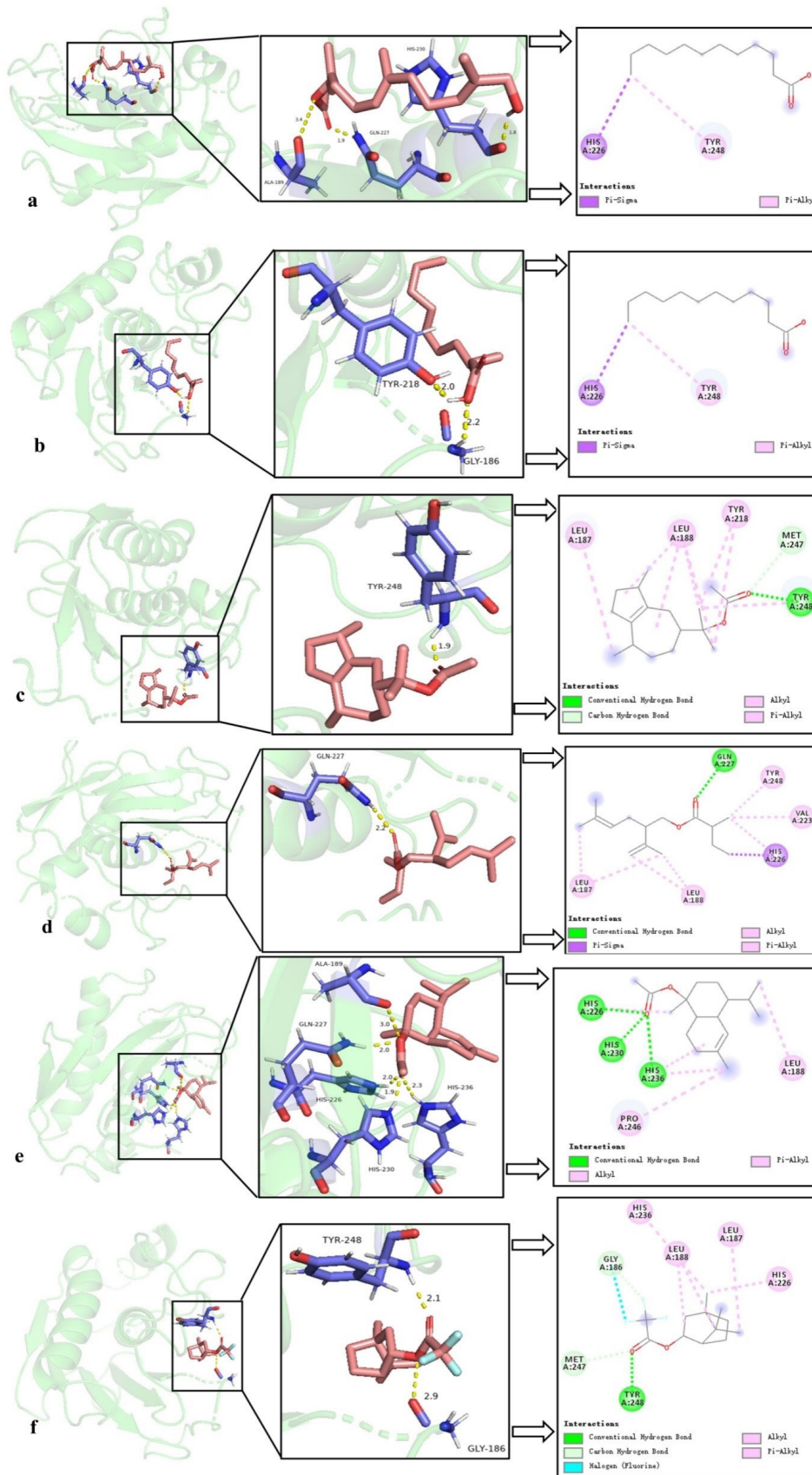


Figure 11. Molecular docking mode. (a) 2,6,10-trimethyl-12-acetoxy-2,6,10-dodecatriene-1-ol- MMP9; (b) dodecanoic acid-MMP9; (c) guaiaol acetate-MMP9; (d) (R)-lavandulyl (R)-2- methylbutanoate-MMP9; (e) tau-cadinol acetate-MMP9; (f) trifluoroacetyl-episoborneo -MMP9.

to have good antioxidant properties (Mett & Müller, 2021; Mett, 2021). In addition, dodecanoic acid can also enhance mitochondrial respiration and glycolysis in cardiomyocytes, as well as suppress inflammatory gene expression (Venkatesan et al., 2022). The concentration of capric and dodecanoic acids were high in our 10 batches of MFO, ranging from 33.77%~90.86% of the total fatty oil. Migao is thus projected to be a new source of natural medications for the treatment of OD-CHD.

With the use of GC-MS, the chemical composition of MFO was determined, and data from the OD-CHD public database was combined. Network pharmacology was used to predict the potential targets and mechanisms of MFO in the treatment of OD-CHD. The top five targets of MFO in the treatment of OD-CHD were AKT1, TNF, EGFR, PTGS2, and MMP9. Pathway analysis showed that MFO mainly regulated lipids and atherosclerosis, PI3K-Akt occurs in the signalling pathway, Rap1 signalling pathway, and MAPK signalling pathway, and the fluid shear stress that influences atherosclerosis and other pathways may be targeted to treat OD-CHD.

Through the analysis of core genes and main pathways, MFO may be involved in the oxidation process, inflammatory response, endothelial dysfunction and other processes, to play a role in the treatment of OD-CHD. For example, AKT1 was the major AKT isoform in the heart and blood vessels, and the activation of AKT1 was associated with inflammation, oxidative stress, accumulation of oxidized lipids, and formed a positive feedback loop exacerbating the consequences of oxidative stress. Interfering with Akt1 signalling *in vivo* may therefore protect and improve survival under dyslipidaemia by reducing oxidative stress and the response to oxidized lipids (Wang et al., 2022a; Hu et al., 2020). Atherosclerosis is a chronic inflammatory condition in which lipid-rich plaques in the walls of arteries result in constriction. Elevated levels of low-density lipoprotein cholesterol (LDL) constitute major risk factors for atherosclerosis (Lau et al., 2021). LDL is oxidatively modified and accumulates in blood vessel walls. Oxidized low-density lipoprotein is involved in the production of adhesion molecules and the recruitment of monocytes to the subendothelial region, affecting oxidative stress, inflammation, and endothelial dysfunction. Monocytes multiply and develop into macrophages, hastening plaque formation, local inflammation, and thrombosis (Jia et al., 2022; Xiong et al., 2022). Therefore, for prevention, lipid aggregation and oxidation must be avoided. The vascular physiology and pathobiology of the vessel wall are influenced by fluid shear stress (FSS) acting on the vessel lumen. FSS has been shown to prevent the formation of atherosclerotic plaques by boosting endothelial denudation and vascular smooth muscle cell production, as well as upregulating endogenous antioxidant genes (Psefteli et al., 2018).

Rap1 is a member of the Ras family of small GTPases, and its activation improves vascular barrier function (Yamamoto et al., 2021). Rap1 mainly promotes nitric oxide release during laminar flow and mostly suppresses pro-inflammatory signals in the absence of laminar flow, hence guarding against atherosclerosis (Singh et al., 2021). Rap1 deficiency causes excessive nicotinamide adenine dinucleotide phosphate (NADPH) oxidase activation and increased production of large reactive oxygen species. As a

result, intervening in the Rap1 signalling pathway can help prevent atherosclerosis (Wong et al., 2018).

MFO may play a role in the therapy of OD-CHD by interfering with the pathways and targets mentioned above, as predicted by network pharmacology. This suggests that MFO can help OD-CHD by interacting with a variety of targets and pathways.

5 Conclusions

In this study, the anti-oxidative efficacy of MFO was confirmed using *in vitro* antioxidant tests, the chemical components of MFO were identified using GC-MS, and its mechanism of action in the treatment of OD-CHD was investigated using network pharmacology. The findings suggested that MFO treatment of OD-CHD had multi-component, multi-target, and multi-pathway characteristics, implying that oxidative stress, inflammatory response, endothelial dysfunction, and other processes might be involved. Further research into the mechanism of action of MFO in the treatment of OD-CHD is needed, and our findings will help.

Ethical approval

Not applicable. No studies in humans or animals have been carried out.

Conflict of interest

All authors have no relevant relationships to disclose.

Funding

This work was financed by the National Nature Science Foundation of China - Guizhou Provincial People's Government Joint Fund (No.U1812403-2), co-financed by Guizhou Provincial Science and Technology Projects [ZK[2022] 463] and Guizhou Province Postgraduate Research Fund Project (YJSKYJJ [2021] 164).

Author contributions

Lina Jian: conceptualization, Writing-original draft, visualization. Jiangtao Guo: conceptualization, writing-original draft, supervision, funding acquisition. Yongping Zhang: writing-review & editing, funding acquisition. Jie Liu: conceptualization, writing-review & editing, supervision, funding acquisition. Yao Liu: writing-review & editing. Jian Xu: writing-review & editing, supervision, funding acquisition.

References

- Aljobair, M. O. (2022). hemical composition, antimicrobial properties, and antioxidant activity of galangal rhizome. *Food Science and Technology (Campinas)*, 42, e45622. <http://dx.doi.org/10.1590/fst.45622>.
- Chen, X., Li, X., Xu, X., Li, L., Liang, N., Zhang, L., Lv, J., Wu, Y. C., & Yin, H. (2021). Ferrotosis and cardiovascular disease: role of free radical-induced lipid peroxidation. *Free Radical Research*, 55(4), 405-415. <http://dx.doi.org/10.1080/10715762.2021.1876856>. PMID:33455488.

- Gatasheh, M. K., Malik, A., Ola, M. S., & Alhomida, A. S. (2021). Photo-activated proflavine degrades protein and impairs enzyme activity: involvement of hydroxyl radicals. *Toxicology Reports*, 9, 78-86. <http://dx.doi.org/10.1016/j.toxrep.2021.12.009>. PMID:35024344.
- Gebicki, J. M., & Nauser, T. (2021). Initiation and prevention of biological damage by radiation-generated protein radicals. *International Journal of Molecular Sciences*, 23(1), 396. <http://dx.doi.org/10.3390/ijms23010396>. PMID:35008823.
- Halliwell, B. (2020). Reflections of an aging free radical. *Free Radical Biology & Medicine*, 161, 234-245. <http://dx.doi.org/10.1016/j.freeradbiomed.2020.10.010>. PMID:33059021.
- Halliwell, B., Adhikary, A., Dingfelder, M., & Dizdaroglu, M. (2021). Hydroxyl radical is a significant player in oxidative DNA damage in vivo. *Chemical Society Reviews*, 50(15), 8355-8360. <http://dx.doi.org/10.1039/D1CS00044F>. PMID:34128512.
- Hu, C. T., Shao, Y. D., Liu, Y. Z., Xiao, X., Cheng, Z. B., Qu, S. L., Huang, L., & Zhang, C. (2021). Oxidative stress in vascular calcification. *Clinica Chimica Acta*, 519, 101-110. <http://dx.doi.org/10.1016/j.cca.2021.04.012>. PMID:33887264.
- Hu, X., Li, B. J., Li, L. C., Li, B. W., Luo, J. L., & Shen, B. (2020). Asiatic acid protects against doxorubicin-induced cardiotoxicity in mice. *Oxidative Medicine and Cellular Longevity*, 2020, 5347204. <http://dx.doi.org/10.1155/2020/5347204>. PMID:32509145.
- Huang, K., Liu, J., Huang, C. H., Liu, Y., Chen, C., Zhang, Y. P., & Xu, J. (2020). Comparative analysis of volatile oil and fatty oil constituents from *Cinnamomum migao* in different sources. *China Pharmacy*, 31(16), 1961-1966.
- Jia, J., Wang, Y. P., Huang, R. J., Du, F. X., Shen, X. Z., Yang, Q. R., & Li, J. (2022). Protein disulfide-isomerase A3 knockdown attenuates oxidized low-density lipoprotein-induced oxidative stress, inflammation and endothelial dysfunction in human umbilical vein endothelial cells by downregulating activating transcription factor 2. *Bioengineered*, 13(1), 1436-1446. <http://dx.doi.org/10.1080/21655979.2021.2018980>. PMID:34983301.
- Jovanović, A. A., Djordjević, V. B., Petrović, P. M., Pljevljakušić, D. S., Zdunić, G. M., Šavikin, K. P., & Bugarski, B. M. (2021). The influence of different extraction conditions on polyphenol content, antioxidant and antimicrobial activities of wild thyme. *Journal of Applied Research on Medicinal and Aromatic Plants*, 25, 100328. <http://dx.doi.org/10.1016/j.jarmp.2021.100328>.
- Lau, K.-K., Chua, B. J., Ng, A., Leung, I. Y.-H., Wong, Y.-K., Chan, A. H.-Y., Chiu, Y.-K., Chu, A. X.-W., Leung, W. C. Y., Tsang, A. C.-O., Teo, K.-C., & Mak, H. K.-F. (2021). Low-density lipoprotein cholesterol and risk of recurrent vascular events in chinese patients with ischemic stroke with and without significant atherosclerosis. *Journal of the American Heart Association*, 10(16), e021855. <http://dx.doi.org/10.1161/JAHA.121.021855>. PMID:34369170.
- Li, S., Duan, X. T., Wang, Q. Y., Liu, J. X., He, T. M., Zhang, J. Y., & Li, X. F. (2022). Mechanisms underlying the activity of paederus in hepatocellular carcinoma: a network pharmacology and *in vitro* validation approach. *Pharmacological Research - Zhongguo Xiandai Zhongyao*, 3, 100089.
- Li, Y. H., & Yang, X. (2021). Protective effect of *Cinnamomum migao* in GuiZhou on acute myocardial ischemia injury. *Information on Traditional Chinese Medicine*, 37(3), 4-8.
- Liang, L., Wen, L., Weng, Y., Song, J., Li, H., Zhang, Y., He, X., Zhao, W., Zhan, M., Li, Y., Lu, L., Xin, Y., & Lu, C. (2021). Homologous-targeted and tumor microenvironment-activated hydroxyl radical nanogenerator for enhanced chemioimmunotherapy of non-small cell lung cancer. *Chemical Engineering Journal*, 425, 131451. <http://dx.doi.org/10.1016/j.cej.2021.131451>.
- Liu, W., Zhang, X., Ma, T., Wang, J., Lv, X., Wu, B., Yan, T., & Jia, Y. (2022). Uncovering the pharmacological mechanism of Wei-Tong-Xin against gastric ulcer based on network pharmacology combined with *in vivo* experiment validation. *Journal of Ethnopharmacology*, 293(July), 115282. <http://dx.doi.org/10.1016/j.jep.2022.115282>. PMID:35405254.
- Mett, J. (2021). The impact of medium chain and polyunsaturated ω -3-fatty acids on amyloid- β deposition, oxidative stress and metabolic dysfunction associated with alzheimer's disease. *Antioxidants*, 10(12), 1991. <http://dx.doi.org/10.3390/antiox10121991>. PMID:34943094.
- Mett, J., & Müller, U. (2021). The medium-chain fatty acid decanoic acid reduces oxidative stress levels in neuroblastoma cells. *Scientific Reports*, 11(1), 6135. <http://dx.doi.org/10.1038/s41598-021-85523-9>. PMID:33731759.
- Nie, X., Wang, Z., Ren, J., Liu, X., Xu, Z., Whang, W., Liang, Z., Mans, D., & Zhang, X. (2022). Identification of antioxidant ingredients by GC-MS from the essential oil of Purple *Eleutherococcus simonii* leaves. *Food Science and Technology (Campinas)*, 42, e76821. <http://dx.doi.org/10.1590/fst.76821>.
- Oh, K., Adnan, M., & Cho, D. (2021). Uncovering mechanisms of *Zanthoxylum piperitum* fruits for the alleviation of rheumatoid arthritis based on network pharmacology. *Biology (Basel)*, 10(8), 703. <http://dx.doi.org/10.3390/biology10080703>. PMID:34439936.
- Panov, A. V., & Dikalov, S. I. (2020). Cardiolipin, perhydroxyl radicals, and lipid peroxidation in mitochondrial dysfunctions and aging. *Oxidative Medicine and Cellular Longevity*, 2020, 1323028. <http://dx.doi.org/10.1155/2020/1323028>. PMID:32963690.
- Psefteli, P., Fowler, M., Mann, G. E., & Siow, R. C. (2018). ECS-7-Redox regulation in human endothelial cells: a critical role for the glycocalyx in mechanotransduction of fluid shear stress. *Free Radical Biology & Medicine*, 120(May), S26. <http://dx.doi.org/10.1016/j.freeradbiomed.2018.04.029>.
- Saifudeen, I., & Renuka, N. (2021). Reactivation of fatty acid oxidation by medium chain fatty acid prevents myocyte hypertrophy in H9c2 cell line. *Molecular and Cellular Biochemistry*, 476(1), 483-491. PMID:33000353.
- Sherratt, S. C. R., & Mason, R. P. (2018). Eicosapentaenoic acid inhibits oxidation of high density lipoprotein particles in a manner distinct from docosahexaenoic acid. *Biochemical and Biophysical Research Communications*, 496(2), 335-338. <http://dx.doi.org/10.1016/j.bbrc.2018.01.062>. PMID:29331380.
- Singh, B., Kosuru, R., Lakshmikanthan, S., Sorci-Thomas, M. G., Zhang, D. X., Sparapani, R., Vasquez-Vivar, J., & Chrzanoska, M. (2021). Endothelial Rap1 (Ras-Association Proximate 1) restricts inflammatory signaling to protect from the progression of atherosclerosis. *Arteriosclerosis, Thrombosis, and Vascular Biology*, 41(2), 638-650. <http://dx.doi.org/10.1161/ATVBAHA.120.315401>. PMID:33267664.
- Sun, J., Wang, H., Cheng, G., Zhang, L., Qu, Z., Han, C., Zheng, W., Wu, L., & Zhang, J. (2022). Revealing the action mechanisms of scutellarin against glioblastoma based on network pharmacology and experimental validation. *Food Science and Technology (Campinas)*, 42, e106121. <http://dx.doi.org/10.1590/fst.106121>.
- Venkatesan, R., Karuppiyah, P. S., Eshwaran, K., Chelladurai, K. B., & Balamuthu, K. (2022). Dual roles of coconut oil and its major component lauric acid on redox nexus: focus on cytoprotection and cancer cell death. *Frontiers in Neuroscience*, 16, 833630. <http://dx.doi.org/10.3389/fnins.2022.833630>.
- Ullah, S., Hasan, Z., Zorriehzahra, M. J., & Ahmad, S. (2017). Diagnosis of endosulfan induced DNA damage in rohu (Labeo rohita, Hamil-

- ton) using comet assay. *Iranian Journal of Fisheries Science*, 16(1), 138-149.
- Wang, L., Zheng, W. Y., Yang, J. X., Ali, A., & Qin, H. (2022a). Mechanism of astragalus membranaceus alleviating acquired hyperlipidemia induced by high-fat diet through regulating lipid metabolism. *Nutrients*, 14(5), 954. <http://dx.doi.org/10.3390/nu14050954>. PMID:35267929.
- Wang, Y., Yuan, Y., Wang, W., He, Y., Zhong, H., Zhou, X., Chen, Y., Cai, X. J., & Liu, L. Q. (2022b). Mechanisms underlying the therapeutic effects of Qingfei Yin in treating acute lung injury based on GEO datasets, network pharmacology and molecular docking. *Computers in Biology and Medicine*, 145, 105454. <http://dx.doi.org/10.1016/j.compbiomed.2022.105454>. PMID:35367781.
- Wei, L., Dong, W. H., Han, Z., Chen, C., Jin, Q., He, J. L., & Cai, Y. P. (2022). Network pharmacologic analysis of *Dendrobium officinale* extract inhibiting the proliferation of gastric cancer cells. *Frontiers in Pharmacology*, 13(March), 832134. <http://dx.doi.org/10.3389/fphar.2022.832134>. PMID:35401206.
- Wong, K. H. K., Cai, Y., Ying, F., Chen, X., Vanhoutte, P. M., & Tang, E. H. C. (2018). Deletion of Rap1 disrupts redox balance and impairs endothelium-dependent relaxations. *Journal of Molecular and Cellular Cardiology*, 115(February), 1-9. <http://dx.doi.org/10.1016/j.yjmcc.2017.12.009>. PMID:29277598.
- Wu, H. B., Xiao, Y. G., Chen, J. S., & Qiu, Z. K. (2022). The potential mechanism of Bupleurum against anxiety was predicted by network pharmacology study and molecular docking. *Metabolic Brain Disease*, 37(5), 1609-1639. <http://dx.doi.org/10.1007/s11011-022-00970-1>. PMID:35366129.
- Xiong, X., Yan, Z., Jiang, W., & Jiang, X. J. (2022). ETS variant transcription factor 6 enhances oxidized low-density lipoprotein-induced inflammatory response in atherosclerotic macrophages via activating NF- κ B signaling. *International Journal of Immunopathology and Pharmacology*, 36. <http://dx.doi.org/10.1177/20587384221076472>. PMID:35306921.
- Yamamoto, K., Takagi, Y., Ando, K., & Fukuhara, S. (2021). Rap1 Small GTPase regulates vascular endothelial-cadherin-mediated endothelial cell-cell junctions and vascular permeability. *Biological & Pharmaceutical Bulletin*, 44(10), 1371-1379. <http://dx.doi.org/10.1248/bpb.b21-00504>. PMID:34602545.
- Yu, Z., Wu, Y., Ma, Y., Cheng, Y. H., Song, G., & Zhang, F. (2022). Systematic analysis of the mechanism of aged citrus peel (Chenpi) in oral squamous cell carcinoma treatment via network pharmacology, molecular docking and experimental validation. *Journal of Functional Foods*, 91(April), 105012. <http://dx.doi.org/10.1016/j.jff.2022.105012>.
- Zhang, J., Li, H. Y., Wang, W., & Li, H. (2022a). Assessing the anti-inflammatory effects of quercetin using network pharmacology and *in vitro* experiments. *Experimental and Therapeutic Medicine*, 23(4), 301. <http://dx.doi.org/10.3892/etm.2022.11230>. PMID:35340883.
- Zhang, L., Zhu, C. Y., Liu, X. Q., Su, E. Z., Cao, F. L., & Zhao, L. G. (2022b). Study on synergistic antioxidant effect of typical functional components of hydroethanolic leaf extract from ginkgo biloba *in vitro*. *Molecules (Basel, Switzerland)*, 27(2), 439. <http://dx.doi.org/10.3390/molecules27020439>. PMID:35056751.
- Zhong, S., Li, L., Shen, X., Li, Q., Xu, W., Wang, X., Tao, Y., & Yin, H. (2019). An update on lipid oxidation and inflammation in cardiovascular diseases. *Free Radical Biology & Medicine*, 144, 266-278. <http://dx.doi.org/10.1016/j.freeradbiomed.2019.03.036>. PMID:30946962.
- Zhu, W., Li, Y. H., Zhao, J. J., Wang, Y. F., Li, Y. X., & Wang, Y. (2022). The mechanism of triptolide in the treatment of connective tissue disease-related interstitial lung disease based on network pharmacology and molecular docking. *Annals of Medicine*, 54(1), 541-552. <http://dx.doi.org/10.1080/07853890.2022.2034931>. PMID:35132912.